# ChemComm

**COMMUNICATION**

# Formation of a porous cerium oxide membrane by anodization†

**Neil J. Lawrence, Keren Jiang and Chin Li Cheung***

**A two-step synthetic process is reported to fabricate porous ceria membranes by anodization of cerium metal foils with subsequent calcination. "Ribbon-like" structures were found to form the backbones of these porous frameworks. The hydrophobic nature of these membranes was revealed by water contact angle measurements.**

Nanoporous membrane structures are potentially suitable for efficient catalytic treatment of reactants because such structures do not aggregate like nanoparticles which have diminished effective catalytic surface areas when used in bulk forms. They can also serve as media for separating reactants and products on different sides of the membranes such as in solid state oxide fuel cells. Anodization is commonly used to synthesize a wide variety of porous films on metal surfaces from metal foils.[1] For examples, nanoporous metal oxide membranes made of titania[2] or alumina[3] can be fabricated by anodizing the corresponding metal foils or films directly to their oxides. Besides oxides, anodization has been applied to convert metal foils such as zinc to either phosphates or similar inorganic adherent compounds on metal substrates.[1a] Nonetheless, exfoliating metal compounds such as cerium oxides and iron oxides have not been fabricated directly by anodization of the corresponding metal foils because thick films of exfoliating compounds can fall off easily from the metal substrates.

Ceria (fluorite structured $CeO_{2-x}$ where $x = 0$ to $0.5$) has recently been attracting much attention in the oxidative catalysis research community due to its high oxygen storage capacity.[4] It has also been used in applications including optical coating and fuel cells[5] because of its high ultraviolet absorbance,[6] high oxygen ion mobility[7] and its multiple valence states.[8] Wide spread of use of cerium compounds in industrial applications is spurred by its large abundance on earth's crust, even more than that of copper.[8,9]

Herein we report a synthetic strategy to fabricate porous membranes composed of exfoliating cerium oxides through creating intermediate adherent hydroxide polymer films by anodization. The rationale behind converting a cerium metal foil to hydroxide polymers is based on the bonding nature

*Department of Chemistry and Nebraska Center for Materials and Nanosciences, University of Nebraska-Lincoln, Lincoln, Nebraska 68588, USA. E-mail: ccheung2@unl.edu; Tel: +1 402-472-5172*
† Electronic supplementary information (ESI) available: Additional materials. See DOI: 10.1039/c0cc04806b

between metal hydroxides and the metal atoms at the metal–hydroxide interface which allows improving the adhesion and build-up of thick metal–hydroxide polymer films. Such hydroxide films can be further converted to oxides by controlled calcination.

In a typical experiment, a cerium metal foil (1 cm², 0.25 mm thick, 99.9% Alfa Aesar, Ward Hill, MA) was anodized at constant current of 100 µA in a two-electrode cell configuration with a platinum cathode to create a porous membrane. The optimal electrolyte solution was composed of 0.15 M ammonium hydroxide ($NH_4OH$) in a mixture of 10% v/v water in ethylene glycol. The sample was considered to be fully anodized once the potential reached 1000 V. Formation of vapor filled "bubbles" (cavities) was observed on the surface of the foil during the entire anodization process. Typically, 160 hours were required to fully anodize the foil sample. The as-anodized sample was bathed in 200-proof ethanol and stirred overnight to remove the ethylene glycol inside the pores. The sample was then calcined in a 1″-tube furnace at 400 °C in a stream of 100 SCCM dry air at 0.1 Torr for 15 h. Experimental details can be found in the ESI.†

Typical scanning electron microscopy (SEM) images of the anodized cerium foil calcined at 400 °C revealed the "ribbon-like" structures forming the backbones of the porous framework (Fig. 1a and b). The average thickness of these "ribbon-like" structures is 24 ± 4 nm. Full anodization of a foil sample is usually found to be split it into two membranes of ≈125 µm in thickness.† Side view SEM images of these membranes indicate that these membranes were composed of channels of pores formed perpendicular to the membrane surface. A transmission electron microscopy (TEM) image and a selected area electron diffraction pattern of one "ribbon-like" structure suggest that the sample calcined at 400 °C is made of highly crystalline ceria (Fig. 1c). A zoomed-in TEM image (Fig. 1d) of the structure shows a lattice fringe pattern with spacing of 0.31 nm, which corresponds to those of a ceria (111) facet.

The crystal structures of the anodized cerium foil and their transformation by calcination were characterized by X-ray diffraction (XRD) (Fig. 2) and indexed against JCPDS data.‡ The XRD pattern of a fully anodized cerium foil suggests that the anodization process transforms the cerium metal foil into $P6_3/m$ hexagonal cerium(III) hydroxide ($Ce(OH)_3$) which oxidizes to $P\bar{3}m1$ hexagonal $Ce_2O_3$. The pattern also indicates the presence of a trace amount of α-Ce metal which implies that some cerium metal may be preserved between the pores
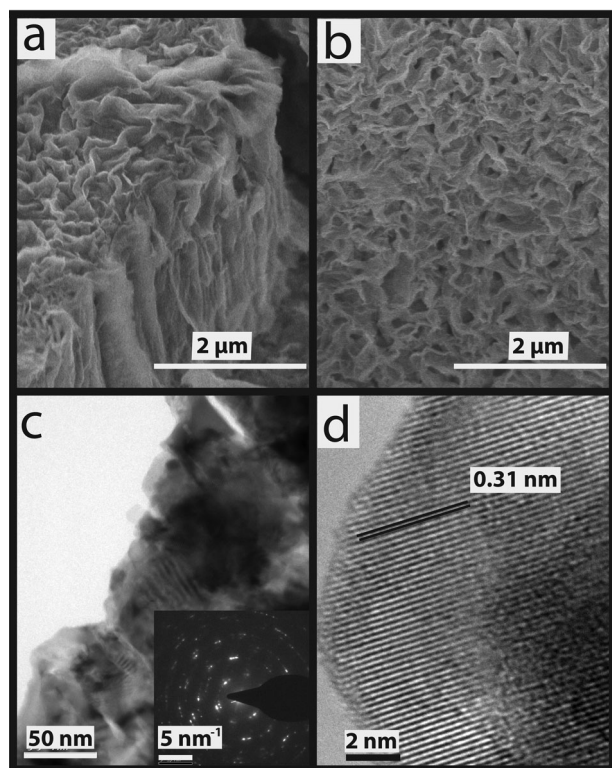
**Fig. 1** Ceria porous membranes made by a two-step anodization–calcination process. (a) Oblique view and (b) top view SEM images illustrate the porous nature of membrane and "ribbon-like" frameworks on the membrane surface. (c) TEM image of a ribbon structure. (inset) SAED pattern. (d) HRTEM image of one piece of the "ribbon-like" framework. The lattice plane spacing is consistent with those of ceria (111) facets.
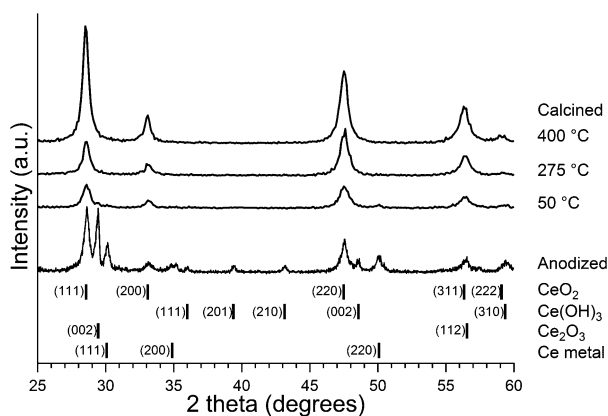


**Fig. 2** XRD patterns showing the transition of as-anodized cerium foils from simple hexagonal cerium(III) hydroxide (Ce(OH)$_3$) to fluorite-structured ceria (CeO$_{2-x}$) as the calcination temperature increases 50, 275 to 400 °C. (bottom) Vertical lines showing peak indexes of CeO$_2$, Ce(OH)$_3$, Ce$_2$O$_3$ and α-Ce from the corresponding JCPDS data.‡

(right figure in Scheme 1). Small isolates of cerium metal are likely located in areas where the hydroxide thickness of the pores limits the oxidation at the applied potential. The presence of peaks indexed to Ce$_2$O$_3$ and CeO$_2$ in the XRD pattern of the as-anodized material indicates that some of the hydroxide undergoes further oxidation during the anodization
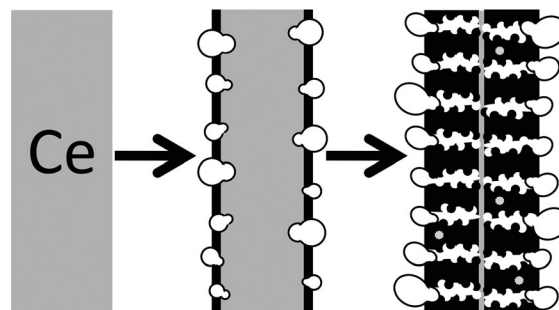


**Scheme 1** Proposed mechanism for the formation of the porous anodized structures from a cerium metal foil. Gray is the cerium metal and black is the anodized complex. The cerium metal acts as the anode in the electrochemical cell. As a complex layer begins to form, vapor filled voids (cavities) or "bubbles" form on the surface and create pathways to the metal, allowing the diffusion of reactants to the metal surface. Pores are formed from volume changes due to the formation of the cerium hydroxide. The formation of gas cavities allow the reaction to continue to completion. Small deposits of unoxidized metal may be left as shown in the final stage of the anodization.

process. The XRD patterns of anodized samples calcined at 50, 275 and 400 °C were also collected to verify the transformation of the anodized samples into cubic $Fm\bar{3}m$ ceria. Compared to the XRD pattern of the as-anodized sample, the relative intensities of diffraction peaks belonging to the cerium hydroxide and metal in the XRD pattern of the sample calcined at 50 °C decrease significantly. For samples calcined at higher temperatures, diffraction peaks of the cubic fluorite structure are dominant in the corresponding XRD patterns. There were no indications of metallic cerium in these patterns. Only the XRD pattern of the sample calcined at 400 °C shows no satellite peaks belonging to Ce(OH)$_3$ and hexagonal Ce$_2$O$_3$, indicating a complete conversion of the sample into fluorite ceria.

Raman scattering spectrum (Fig. S2, ESI†) of the porous CeO$_{2-x}$ membrane displays a peak near 462 cm$^{-1}$, which is typically assigned to the T$_{2g}$ (F$_{2g}$ in some tables)[10] mode of the Ce–O vibrational unit with $O_h$ symmetry.[11] No other significant peaks are found in this spectrum, indicating that the annealed membrane does not have a significant number of lattice related defects.[12]

The effect of the porous structures on the water wettability of the ceria membrane was examined by water contact angle measurements (Fig. S3, ESI†). The apparent advancing water contact angles of 0.25 μl water droplets on the calcined CeO$_{2-x}$ membranes were measured to be 120 ± 4°. Water contact angle measurements were also performed on calcined samples with the porous structures destroyed by sonication in ethanol and on an air-oxidized cerium foil. The corresponding measurements yield values of 31 ± 3° and 17 ± 3°, respectively, suggesting the necessity of porous structures in the apparent hydrophobic nature of the ceria membranes. The Cassie–Baxter model[13] was applied to describe the apparent water contact angle ($\theta_c$) of a textured hydrophobic surface:

$$\cos\theta_c = f_1 \cos\theta_1 + f_2 \cos\theta_2 \qquad (1)$$

where $f_1$ and $f_2$ are the surface area fractions of the membrane for components 1 and 2. The contact angles $\theta_1$ and $\theta_2$ are of water on a smooth surface of components 1 and 2. When the

This journal is © The Royal Society of Chemistry 2011

droplet is water and air is the trapped gas, $\theta_2$ is $180°$, allowing the re-expression of eqn (1) as

$$\cos\theta_c = f_1(\cos\theta_1 + 1) - 1 \qquad (2)$$

Utilizing eqn (2), the area fraction of the solid–water interface for the porous membrane surface $f_1$ is estimated to be *ca.* 0.62. Given that the surface is topographically irregular and it does not contain large changes in the chemical hydrophobicity, the Cassie–Baxter model is adequate to explain our measurements. This fraction correlates well with the average value estimated from SEM images of the membranes (0.51 ± 0.03).†

A multi-stage formation mechanism for the porous anodized cerium foil structures with the "ribbon-like" backbone framework can be deduced from the experimental observations and the possible electrochemical reaction scheme (Scheme 1). In the initial stage of the anodization, the cerium metal was electrochemically oxidized to cerium(III) ions ($Ce^{3+}$). At the metal surface, the formation of soluble complexes ($[Ce(NH_3)_{12-x}](OH)_x$)[14] led to pitting of the metal foil surface. Electric fields enhanced by the high curvatures of the pits possibly caused an increase in the pit size. The $Ce^{3+}$ ions reacted with hydroxide ions to form $Ce(OH)_3$ polymers. The ammonium cations likely complexed with $Ce^{3+}$ ions to form $Ce–NH_3–H_2O$ soluble chemical species. The formation of this complex possibly caused the dissolution of the cerium(III) hydroxide.

An increase in the ammonia concentration of the electrolyte was found to produce a decrease in the density and thickness of the "ribbon-like" structures. The cerium anode simply appeared to dissolve into the electrolyte solution. This was likely caused by the increased formation rate of the soluble ammonia complexes which competed with the precipitation and formation of the cerium hydroxide framework. However, if the concentration of ammonium ions was very low or the ammonium ions were replaced by sodium ions, the cerium oxide was observed to form, and then exfoliate from the cerium foil. Therefore, the concentration of $NH_4^+$ ions is critical to the proper formation of the membrane.

At the surface of the cerium foil, oxygen was produced in the oxidation reaction and cavities (vapor filled bubbles) were observed trapped in the porous matrix during the anodization process. The radius ($r$) of a cavity before it left the surface of a solid is a function of the buoyancy of the trapped vapor ($P_{in}$) being resisted by the pressure of the liquid ($P_{out}$) and the surface tension ($\gamma$) causing the adhesion of the cavity to the solid. The use of an electrolyte with a surface tension much less than that of water favored the formation of smaller cavities as indicated by the Young–Laplace relationship.[15]

$$r = \frac{2\gamma}{P_{in} - P_{out}} \qquad (3)$$

The formation of the low-solubility $Ce(OH)_3$ precipitated around the cavities, leading to the growth of the thin "ribbon-like" structures of the porous framework. As the cavities of trapped gas increased in size, they eventually escaped, leaving voids adjacent to the bare metal and allowing the continuation of the anodization process.

Current density appears to affect the growth rate of the "ribbon-like" structures. At a fixed current, the thickness of the cerium hydroxide porous structures increased at a constant rate. An increase or decrease in the applied current was found to change the film growth rate proportionally. The pore size was observed to increase with an increase in current density (data not shown). Similar to the case of anodizing porous silicon, once a threshold current level was reached, the pore diameters of the anodized structures became too large that a smooth surface was obtained instead.[16]

In conclusion, a two-step synthetic strategy has been successfully demonstrated to fabricate porous membranes of cerium oxide that does not exfoliate. The reported strategy has the potential to lead to scientific and commercial progress in the fabrication of protective coatings and porous membranes made of oxides which would otherwise exfoliate.

## Notes and references

‡ Joint Committee on Powder Diffraction Standards (JCPDS) cards 00-008-0056 αCe *Fm$\bar{3}$m*, 00-034-0394 CeO$_2$ *Fm$\bar{3}$m*, 01-074-0665 Ce(OH)$_3$ *P6$_3$/m* and 00-023-1048 Ce$_2$O$_3$ *P$\bar{3}$m1*.

1 (a) S. Wernick, *The surface treatment and finishing of aluminum and its alloys*, Finishing Publications Ltd, ASM International, Metals Park, 5th edn, 1987; (b) G. Butail, P. G. Ganesan, M. Raddiar, R. Teki, N. Ravishankar, D. J. Duquette and G. Ramanath, *Thin Solid Films*, 2010, DOI: 10.1016/j.tsf.2010.10.004.
2 K. Lee, D. Kim, P. Roy, I. Paramasivam, B. I. Birajdar, E. Spiecker and P. Schmuki, *J. Am. Chem. Soc.*, 2010, **132**, 1478–1479.
3 X. Fang, M. Ryan, J. Riley and P. Mason, *Nanotechnology*, 2009. IEEE-NANO 2009, 9th IEEE Conference, 2009.
4 C. T. Campbell and C. H. F. Peden, *Science*, 2005, **309**, 713–714.
5 E. P. Murray, T. Tsai and S. A. Barnett, *Nature*, 1999, **400**, 649–651.
6 P. Maestro and D. Huguenin, *J. Alloys Compd.*, 1995, **225**, 520–528.
7 M. Nolan, J. E. Fearon and G. W. Watson, *Solid State Ionics*, 2006, **177**, 3069–3074.
8 D. Lide, *CRC Handbook of Chemistry and Physics*, CRC, 88th edn, 2007.
9 (a) T. J. Ahrens, *Global earth physics: a handbook of physical constants*, American Geophysical Union, Washington, D.C., 1995; (b) N. Hickey, P. Arneodo Larochette, C. Gentilini, L. Sordelli, L. Olivi, S. Polizzi, T. Montini, P. Fornasiero, L. Pasquato and M. Graziani, *Chem. Mater.*, 2007, **19**, 650–651.
10 D. C. Harris and M. D. Bertolucci, *Symmetry and spectroscopy: an introduction to vibrational and electronic spectroscopy*, Dover Publications, New York, 1989.
11 B. P. Mandal, V. Grover, M. Roy and A. K. Tyagi, *J. Am. Ceram. Soc.*, 2007, **90**, 2961–2965.
12 T. Taniguchi, T. Watanabe, N. Sugiyama, A. K. Subramani, H. Wagata, N. Matsushita and M. Yoshimura, *J. Phys. Chem. C*, 2009, **113**, 19789–19793.
13 (a) G. McHale, *Langmuir*, 2007, **23**, 8200–8205; (b) L. Gao and T. J. McCarthy, *Langmuir*, 2007, **23**, 3762–3765; (c) E. Hosono, S. Fujihara, I. Honma and H. Zhou, *J. Am. Chem. Soc.*, 2005, **127**, 13458–13459; (d) A. B. D. Cassie and S. Baxter, *Trans. Faraday Soc.*, 1944, **40**, 546–551.
14 B. E. Douglas, D. H. McDaniel and J. J. Alexander, *Concepts and models of inorganic chemistry*, Wiley, New York, 3rd edn, 1994.
15 P. Atkins, *Physical chemistry*, W.H. Freeman and Co., New York, 8th edn, 2005.
16 X. G. Zhang, *J. Electrochem. Soc.*, 2004, **151**, C69–C80.